THEORETICAL AND EXPERIMENTAL INVESTIGATION OF THE PHYSICS OF CRYSTALLINE SURFACES

Principal Investigator: E. Bauer

Annual Report
For the Period 1 February 1968 - 31 January 1969

Prepared for the
National Aeronautics and Space Administration
Washington, D. C.

Fund Transfer R-05-030-001

Naval Weapons Center
China Lake, California 93555

ANNUAL REPORT ON FUND TRANSFER NO. R-05-030-001 FOR THE PERIOD 1 FEBRUARY 1968 THROUGH 31 JANUARY 1969

I. SUMMARY OF WORK

The major effort during the past year was concentrated on the following problems:

(1) The relation between structure of epitaxial films and surface and interfacial energies.

(2) Quantitative studies of the elastic and inelastic interactions of slow electrons with tungsten single crystal surfaces.

(3) The determination of nature and structure of surface layers with low energy electron diffraction.

(4) The relation between structure and electron emission properties of work function reducing layers on tungsten {110} planes.

II. The relation between the structure of epitaxial films and surface and interfacial energies (A. K. Green and E. Bauer)

Several specific problems concerned with the growth of face-centered cubic metals on alkali halide cleavage planes have been studied during the past year.

(1) A wide variety of impurity effects were reported in the first quarterly report and are in press at this time (see VI-3). Among the impurity influences which have been studied are: doped substrates, the surface layer resulting from cleavage in air, residual gas components; ions originating from the vapor source and electron bombardment of the substrate. An understanding of these parameters and how they affect the formation of a film is basic to a complete analysis of film nucleation and growth.

For details of the experiments we refer to the first quarterly report and reference VI-3. Each of the indicated parameters has a significant influence on film formation and must be considered in the analysis of experimental results.

(2) A significant effort was made to obtain a reproducible cleavage surface structure on sodium chloride, for both cleavage in air and in vacuum. This capability is essential to any systematic quantitative study of nucleation processes. The surface structure of the substrate is revealed by the decoration of steps by a thin ($\sim$ 1 Å) gold film. We found that reproducible air-cleaved surfaces could be obtained by careful exposure of the freshly cleaved surface to a controlled humidity (46% R.H.) for a definite time (5 minutes). Cleavage surfaces produced in vacuum are more difficult to control. The surface structure depends on many parameters, e.g., source of crystal, shape and size of crystal, geometry of cleaving mechanism, and crystal temperature during cleavage, to name a few. We have found that Optovac sodium chloride produces better cleavage surfaces (fewer steps) than does Harshaw. Also, a high ratio of width to length along the cleaving direction improves the cleavage surface.

(3) The influence of point imperfections (F-centers) on the epitaxy of gold on NaCl, as reported by T. Inuzuka and R. Ueda, Appl. Phys. Letters 13, 3 (1968), stimulated a series of experiments to verify and understand their observation. In spite of strong efforts to reproduce the reported experimental conditions we were unable to find an influence of F-centers. The possibility remains of some unknown parameter (photons, residual gas, etc.) producing the effect when combined with F-centers. Additional experiments are being considered.

(4) The formation of multiply twinned particles (MTP) as a function of thickness, deposition rate and specimen temperature was also studied. This phenomena has been attributed to both coalescence and to nucleation. By depositing films of equal thickness (1 Å) at various rates we determined that slow rates (< 0.03 Å/sec) produced no MTP but that high rates (0.3 Å/sec) did produce MTP. It was also determined that extremely thin films (~ 0.1 Å) exhibited no MTP down to unexpectedly low temperatures (100°C). These results indicate strongly that MTP is not a nucleation phenomena but most probably is a result of coalescence. Experiments to date have not been exhaustive but have bracketed areas where careful systematic data will produce significant results.

(5) Simultaneous deposition of gold on different alkali halides has revealed large differences in the condensation coefficient. For example, the condensation coefficient for gold on LiF is approximately a factor of ten lower than that for gold on KI. When the reason for this phenomena is understood it may help explain some of the specific differences in film formation on different substrates. The difference in condensation coefficient may be due to differences in the heat of adsorption or possibly to a difference in thermal accommodation resulting from the mass ratios of incident atom/substrate atom. Results to date do not allow ruling out either one. More experiments are being planned to obtain data which will enable understanding of this phenomena.

III. Quantitative studies of the elastic and inelastic interactions of slow electrons with tungsten single crystal surfaces (J. O. Porteus)

Much experimental information has been obtained on elastic and quasi-elastic diffraction of low energy electrons by crystalline surfaces. However, mainly because of the limitations of conventional display-type diffractometers, very little is known about the diffraction of inelastically scattered electrons. Knowledge of the inelastic scattering behavior is not only essential to the complete understanding of elastic diffraction, but may also provide much needed complementary information for the determination of surface structures. Also, an additional important source of information on electronic excitations of solids is provided. A tungsten (110) surface was chosen for the initial study for the following reasons: (1) Two intense, well-resolved characteristic loss maxima are observed in the energy spectrum of the total inelastic scattering; (2) a simple elastic diffraction pattern characteristic of the clean bulk material is easily produced; and (3) a simple and reasonably well defined diffraction pattern representative of a half monolayer of oxygen coverage is also easily obtained. The electronic excitations (band structure) of tungsten are not as simple as that of some other materials, but in view of the above experimental advantages this was felt to be of secondary importance. Measurements consist of retarding field

scans of emerging electron energy distributions in a programmed sequence of adjacent primary energies and emerging angles. Comparison of the intensities of the characteristic loss features in these distributions permits a mapping of intensity maxima on an angle vs. energy plot in any given azimuth. When the energy coordinate in such a plot refers to the emerging or secondary electron energy the maxima corresponding to the two different loss features are generally found to coincide. Moreover, the positions and intensities of the maxima for clean tungsten are roughly as would be expected on the basis of a tandem process of coherent inelastic scattering followed by conventional low energy diffraction. Preliminary results on the oxygen covered surface tend to confirm this picture if extra observed maxima are attributable to the interaction of the inelastic scattering cone with adjacent azimuths (see encl. 1). Although the tandem model provides a crude explanation of results, details of the positions and intensities of maxima are often significantly at variance with this model. Further work is needed to explain these anomalies and to relate them to the areas of theoretical interest.

IV. Determination of nature and structure of surface layers with low energy electron diffraction (F. Bauer)

It is well known now that the electron diffraction patterns of "clean" surfaces of many crystals show a lateral periodicity different from that of the bulk of the crystal. For the interpretation of such patterns it is essential to have information on the chemical composition of the surface, to understand the formation mechanism of the patterns and to have an understanding of the interaction mechanism of the electron beam with the crystal. Of particular importance is the understanding of the influence of inelastic scattering on the penetration depth of the electron beam, because inelastic scattering determines ultimately the thickness of the surface layer which contributes to the (elastic) diffraction pattern. With these objectives in mind the Si(111) surface was chosen for the following reasons: (1) The "clean" Si(111) surface produces several different diffraction patterns depending upon pretreatment; (2) The electronic energy band structure of silicon is well known. Therefore, it can be expected that the inelastic scattering due to single electron interband transitions can be explained in terms of the electronic energy band structure of the crystal; (3) The collective electron excitations (plasmons) in silicon are known to be free-electron gas-like. This is a consequence of the large energy separation of the valence band which contains the four "free" electrons from the next lower energy level (L level); and, (4) Silicon does not alloy with many metals and provides, therefore, an ideal substrate for metal films for the study of the inelastic scattering of slow electrons by metals.

The problems studied and the results obtained during this report period are as follows:

(1) The chemical nature of the Si(111) surfaces exhibiting complex electron diffraction patterns, as determined by Auger electron spectroscopy, low energy electron diffraction and mass spectrometry. The 7x7, $\sqrt{19}$ x $\sqrt{19}$ R(23.5°) structures on the "clean" annealed surface, and the 8x8 structure formed upon heating in NH_3 were studied in considerable detail. The measurements established that

the 7x7 structure is due to a Fe-containing surface layer with Fe_5Si_3 structure, that the $\sqrt{19}$ x $\sqrt{19}$ R(23.5°) structure contains Ni (see VI-3,4) and that the 8x8 structure cannot be ascribed to a Si_4N_3 layer.

These results depend critically on the interpretation of Auger electron spectra, which are very sensitive to the experimental setup. Considerable effort was, therefore, made to optimize the setup and to eliminate artifacts. Towards the end of the report period an experiment was begun to examine the validity of an important implicit assumption which is usually made in the interpretation of Auger electron spectra. This assumption says that Auger electron emission is isotropic, i.e., independent of the orientation of the incident beam with respect to the collector, but depends only upon the inclination of the incident beam with respect to the crystal. Preliminary results indicate that this is not true.

(2) The kinetics of formation of the Si(111) - 7x7 and Si(111) - $\sqrt{19}$ x $\sqrt{19}$ R(23.5°) LEED patterns, previously ascribed to the clean surface. The problem was studied by measuring the intensities, I, of characteristic spots in the LEED pattern as function of distance, x, from the crystal supports after various heating times, t, and temperatures, T. The results show clearly that in the case of the Si(111) - 7x7 pattern I(x,t,T) can be described by a one-dimensional diffusion equation with the crystal mount as source. The measurements were performed in the temperature range from about 700° to 800°C, in which the diffusion coefficient D_s varies from .5 to $4 \cdot 10^{-4}$ $cm^2 sec^{-1}$. From the temperature dependence of D_s an activation energy of 50 kcal/mole follows. The large value of D_s excludes volume diffusion but is compatible with a surface diffusion mechanism. The $\sqrt{19}$ x $\sqrt{19}$ R(23.5°) pattern, however, is formed both by surface and volume diffusion, at least in the crystal investigated which previously had been doped with Ni. Due to the mixed diffusion and the unfavorable geometry of the crystal no diffusion parameters could be determined in this case. Nevertheless, the experiments clearly indicate that both the $\sqrt{19}$ x $\sqrt{19}$ R(23.5°) and 7x7 LEED patterns are formed by diffusion processes of impurities (Ni and very likely Fe, respectively, according to Auger electron spectroscopy) from the bulk and/or from the crystal mount to the crystal surface. This strongly supports the previously proposed surface impurity layer interpretation of the LEED patterns (see above).

(3) The energy loss spectrum of slow electrons (30-150 eV energy) scattered from Si(111) surfaces. The purpose of these measurements was a) to obtain an understanding of the energy loss mechanisms of slow electrons in crystals in terms of single electron transitions and plasmon excitations; and b) to determine the influence of the surface structure on the energy loss spectrum. The experiments were performed for various angles of incidence (θ,ϕ) onto the crystal; the electron current scattered backward into a cone of 90° was energy-analyzed with an energy resolution of .8 eV. The more significant results are as follows: a) the energy distribution from below 0 to about 10 eV energy loss shows considerable structure which changes with θ and ϕ and to a lesser degree with the surface structure. It can be explained in terms of nondirect transitions between the valence and conduction bands of bulk Si (see encl. 2); b) the surface plasmon excitation in Si at about 10.5 eV is abnormally low irrespectively of the surface

structure; it increases only slightly with the polar angle of incidence θ; and c) the threshold for volume plasmon excitation in Si is considerably higher than predicted by theory assuming that the four valence electrons per atom contribute to the "free electron gas". These results clearly indicate the need for a more sophisticated theory and more detailed measurements which are planned.

(4) The energy loss spectrum of slow electrons (30-50 eV) energy scattered in epitaxial Al films on Si(111) surfaces. The purpose of these measurements was to determine whether the abnormalities in the plasmon excitation in Si by slow electrons were typical for Si or a general aspect of plasmon excitation by slow electrons. The Al films were deposited in situ and grew parallel to the substrate, i.e., with a (111) orientation. The measurements were performed as in Problem (3). The most important results are: a) surface plasmon excitation in Al is much stronger than the volume plasmon excitation as expected from theory; this is in strong contrast to Si where the reverse is true; b) the threshold for volume plasmon excitation is much larger than predicted by theory assuming that each atom contributes three electrons to the "free electron gas"; this is in agreement with Si; and c) the energy dependence of the probability for surface plasmon excitation shows an abnormality near the threshold for volume plasmon excitation. The comparison of these results with those listed under (3) clearly demonstrates the poor theoretical understanding of the inelastic scattering of slow electrons at present, even for surfaces which are "simple" from the point of view of collective electron behavior and points out the need for detailed experimental work to help obtain a better understanding.

V. The relation between structure and electron emission properties of work function reducing layers on W(110) surfaces (G. Turner and E. Bauer)

During the last year our effort has been divided into two main areas: (A) Continued development of the ultrahigh vacuum electron microscope (UHVEM); (B) A preliminary study of the interaction of oxygen and carbon monoxide with a W(110) single crystal.

The major effort in area (A) has been the conversion of the UHVEM from a straight beam to a bent beam system. The separation of the illuminating beam from the imaging beam by a magnetic deflection field (bent beam system) allows the filtering of inelastically scattered electrons in the image while, at the same time, not reducing the intensity of the illuminating beam. This will permit us to combine low energy electron microscopy (LEEM) and low energy electron diffraction (LEED) with emission and mirror microscopy and to obtain quantitative information concerning adsorbate influence on surface structure and work function changes.

The bent beam conversion, however, lead to many problems which may, in general, be categorized as follows: (1) System alignment, (2) Image distortion, and (3) Image intensity. The system alignment problems become especially severe in regions of low electron energy such as the objective and filter lens. In these areas, the electrons have an energy of only a few electron volts and any extraneous magnetic fields, for example, must be reduced to a value such that their effect on the beam trajectory becomes sufficiently small. The deflection

pole pieces and yoke were redesigned to minimize the stray field in the area of the objective lens. A further reduction, by a factor of 30, of the magnetic field in this area has been accomplished by the use of modified Helmholtz coils. The total horizontal component of the magnetic field in the specimen area is now about 10 milligauss maximum. The filter lens, which operates at the second magnification maximum, is very sensitive to the mechanical alignment of the center electrode with respect to the optical axis. The center electrode motion control was modified to provide more positive and reproducible positioning. These improvements have resulted in easier and more rapid alignment.

The image distortion, introduced by the 60° deflection field, has been compensated for by use of a single quadrupole lens placed in the imaging column. The residual and stray magnetic fields associated with this quadrupole lens, however, manifest further problems in beam alignment. This problem is still being investigated.

The problem of achieving sufficient image intensity at high magnifications has been approached in three ways: (1) A field-emission electron gun has been designed as a source for the illuminating beam. The field-emission source is over a thousand times brighter than a thermionic emitter and hence provides a much higher beam luminosity. Also, the energy spread is about 0.2 eV for the field emitter as compared to ~ 1 eV for the thermionic emitter operated in the space charge region. The field-emission gun is completed and ready for testing; (2) An electron channel multiplier will be internally mounted adjacent to the fluorescent screen to provide image intensification. An electron gain of $>10^3$ is expected. The mounting hardware is completed and ready for installation and testing; (3) A 3-stage image intensifier combined with a T.V. vidicon has been externally mounted at the viewing screen. The microscopy and diffraction patterns can be viewed on an 8" x 11" monitor. In addition to image intensification and easier alignment, an added degree of image magnification and electronic read-out capability (video tape) is provided.

The investigation of the interaction of oxygen and carbon monoxide with a W(110) single crystal surface was undertaken in an effort to better understand gas-metal surface interactions. The many discrepancies found in literature show the need for more basic investigation of simple, well defined systems such as the system O/W(110). For example, there is little agreement over the oxygen coverage necessary to produce an oxygen-saturated W(110) surface or over the coverage required for the p(2x1) or p(2x2) structures. Disagreements are also found in the values of the work function associated with the formation of the p(2x1) and p(2x2) structures and in the shape of the work function versus oxygen exposure curve. The nature of the adsorbate-substrate bond--whether a simple chemisorption process or one of surface reconstruction--is an equally important question that needs clarifying.

The experiment was set up in a Varian LEED system with a base pressure of 3×10^{-10} Torr. A W(110) single crystal, 9 mm in dia. and 0.15 mm thick, resistively heated, was cleaned in O_2 ($p = 2 \times 10^{-7}$ Torr) at temperatures up to 2300°K for several hours to remove carbon. The source for oxygen deposition was an oxidized W ribbon which provided very reproducible doses of tungsten

oxide (W-O). The change in work function ($\Delta\Phi$) of the W(110) surface upon oxygen adsorption was measured by the retarding field method. A spot photometer was used to measure diffraction spot intensities during deposition. During the oxygen deposition, LEED spot intensity and $\Delta\Phi$ measurements, the pressure was in general 4-6 x 10^{-10} Torr.

It is premature to draw definite conclusions from this experiment at this time. However, some comparisons can be made with other results. In agreement with others[1,2] and our own previous work, we find that upon adsorption of oxygen at room temperature the W(110) surface passes through three distinct stages with increasing coverage: from a clean W(110), p(1x1), (1) to a p(2x1), (2) then to a p(2x2), and finally, (3) to a p(1x1) oxygen-covered W(110). The total work function change, $\Delta\Phi$, is about 1.05 eV for the saturated O_2-covered surface which is in qualitative agreement with others.[2-4] However, the reported O_2 exposure needed to reach saturation varies considerably, e.g., Madey and Yates[4] report a 20,000L O_2 exposure [L = 1 Langmuir = 1 x 10^{-6} Torr/sec] for a change in Φ of 1.2 eV with Φ still increasing. Tracy's[2] results, on the other hand, indicate saturation at about 25L with a change in Φ of about 1 eV.

To relate exposure, L, to coverage, θ, and hence to the number of O_2 atoms on the surface requires a knowledge of the sticking coefficient, S, which can depend upon several factors such as coverage and substrate temperature. If we assume then, as others[1,2] do, that the p(2x1) structure occurs at 1/2 monolayer coverage, we find a $\Delta\Phi$ of about +0.15 to +0.20 eV compared to about +0.68 eV for Tracy.[2] This $\Delta\Phi$ for the 1/2 monolayer occurs at +0.15 to +0.20 eV even for depositions at elevated substrate temperatures up to 1400°K. From Germer's, et al.[1] and our own previous work it is known that at higher oxygen coverage several structures are formed by heating during or after deposition: "c(48 x 16)", "c(21 x 7)" and "c(14 x 7)". The same structures are obtained in the reverse sequence when a crystal saturated with O_2 at room temperature is heated to increasingly higher temperatures resulting in loss of oxygen ("desorption"). The $\Delta\Phi$ associated with the transition between these structures is always a smoothly changing function from zero to maximum coverage independent of whether the structure was obtained by deposition or desorption.

The significant conclusions which can be drawn from this work are: (1) In agreement with Tracy,[2] the $\Delta\Phi$ upon adsorption of oxygen is always a monotonically increasing function and does not exhibit the maximum as reported by Hopkins, et al.[3] (2) In disagreement with Tracy, the $\Delta\Phi$ associated with the p(2x1) structure is very low (.15 - .20 eV), independent of deposition temperature (up to 1400°K). (3) If the reasonable assumption is made that the complex W-O molecules used in our experiment have constant S during the initial stages of deposition, then $\Delta\Phi$ is not a linear function of coverage as deduced by Tracy[2] but strongly depends on oxygen coverage. These conclusions suggest that reconstruction occurs even in the earliest stages of the interaction of oxygen with the W(110) surface.

The study of the interaction of CO with W(110) surfaces was stimulated by two observations made at residual gas pressures of 2-3·10^{-10} Torr on initially clean surfaces: (1) In the UHVEM the photoelectric emission current I_{ph} decreases initially with time, goes through a minimum, and increases again (see Third Quarterly Status Report, Oct. 1967); (2) In the Varian LEED system the work

function as measured with the retarding field method increases up to a maximum of $\Delta\Phi$ = .13 eV and then decreases. When plotted on the same scale the maximum of $\Delta\Phi$ coincides with the minimum of I_{ph}. This suggests a common cause for both effects. These effects seriously hamper experiments with durations of the order of 10 min. or more. Therefore, an effort was made to understand them. The residual gas in both systems consists mainly of H_2 and CO. Only the adsorption of CO was studied.

The W(110) crystal was cleaned and checked by LEED. CO was admitted and the system stabilized at several pressures--2 x 10^{-9} Torr, 8 x 10^{-9} Torr and 4 x 10^{-8} Torr. For each of these pressures the crystal was flashed at 2200°K and $\Delta\Phi$ was measured by the retarding field method and plotted as a function of exposure, L. At the higher pressures our results agree qualitatively with those of Madey and Yates.[4] For exposures > 0.4L, the curve shape is essentially the same with our minimum occurring at about 1.5L compared to 2.2L as reported by Madey and Yates.[4] At low CO pressures (2 x 10^{-9} Torr), however, $\Delta\Phi$ goes through a small maximum at about 0.15L exposure and its height appears to be a function of the CO partial pressure. Also, the depth of minimum at 1.5L exposure decreases with decreasing CO partial pressure.

Hopkins, et al.[3] have reported an initial increase in Φ for hydrogen adsorption on $W(1\bar{1}0)$. Taking this and our residual gas composition into account, the change in I_{ph} and $\Delta\Phi$ of W(110) surfaces exposed to the residual gas can tentatively be explained as follows: initially adsorption of hydrogen causes an increase of Φ; simultaneously, CO is being adsorbed and with increasing coverage is displacing hydrogen, thus reducing Φ. The details of the initial shape of the $\Delta\Phi$(L) curve is determined by the relative partial pressures of hydrogen and carbon monoxide. This has to be kept in mind when the electron emission properties of nearly clean W(110) surfaces are studied at pressures as low as $1 \cdot 10^{-10}$ Torr.

---

1. L. H. Germer, J. W. May, Surface Sci. 4, 452 (1966).
2. J. C. Tracy, Thesis, Cornell University, 1968.
3. B. J. Hopkins, K. R. Pender and S. Usami, Fundamentals of Gas-Surface Reactions, Academic Press (1967), p. 284.
4. T. E. Madey, J. T. Yates, Jr., Supplemento al Nuovo Cimento, 2, 501 (1967).

VI. Publications

1. "Evolution of Water from Alkali Halide Single Crystals" by A. K. Green and E. Bauer, J. Appl. Phys. 39, 2769 (1968).
2. "On the Nature of Annealed Semiconductor Surfaces" by E. Bauer, Phys. Letters 26A, 530 (1968).
3. "The Influence of Impurities on the Formation of Single-Crystal Films" by A. Green, E. Bauer and J. Dancy, "Molecular Processes on Solid Surfaces", edited by E. Drauglis and R. Gretz (McGraw-Hill, N.Y., 1968). In press.
4. "On the Interpretation of Complex LEED Patterns" by E. Bauer, in "The Structure and Chemistry of Solid Surfaces", edited by G. A. Somorjai. In press.

5. "Diffraction of Inelastically Scattered Electrons in Tungsten at Low Energies" by J. O. Porteus, in "The Structure and Chemistry of Solid Surfaces", edited by G. A. Somorjai. In press.

Papers presented

1. "The Influence of Impurities on the Formation of Single Crystal Films" by A. Green, E. Bauer, and J. Dancy. Invited paper at Third Battelle Colloquium on Material Sciences, Kronberg, Germany, 6-11 May 1968.

2. "On the Interpretation of Complex LEED Patterns" by E. Bauer. Invited paper at Fourth International Materials Symposium, Berkeley, California, 19-21 June 1968.

3. "Diffraction of Inelastically Scattered Electrons in Tungsten at Low Energies" by J. O. Porteus. Fourth International Materials Symposium, Berkeley, California, 19-21 June 1968.

Encl. 1

Inelastic Low Energy Electron Diffraction at a Tungsten (110) Surface with Oxygen Coverage

by

J. O. Porteus
Michelson Laboratory, China Lake, California 93555

Although a substantial literature exists on low energy electron diffraction of elastically scattered electrons, the role of diffraction in the attendant inelastic scattering has claimed little attention. Recently it was shown that the scattering of low energy electrons involving characteristic energy loss can be sufficiently coherent to produce pronounced diffraction effects.[1] These effects include well-defined beams of loss electrons having distributions of intensity vs. emerging energy and angle similar to those of corresponding elastic beams. The above work was performed at normal incidence on a clean tungsten (110) surface by measuring the electron energy distribution in its dependence on emerging angle and primary energy in the range 50-200 eV. Measurements have now been extended to include the above surface with an ordered half monolayer of adsorbed oxygen. The present discussion will be based on comparison of elastic and inelastic diffraction features for the oxygen-covered surface with those of clean tungsten. Of special interest is the sensitivity of inelastic diffraction to foreign surface atoms and information on the mean free path for inelastic scattering. Implications for the validity of the tandem models, where diffraction and inelastic scattering are regarded as independent, will be discussed. Measurements at nonnormal incidence, which provide information on the excited states giving rise to the loss beams, will also be presented.

---

[1] J. O. Porteus, in The Structure and Chemistry of Solid Surfaces, Fourth International Materials Symposium (John Wiley and Sons, New York, 1969), to be published.

Inelastic Scattering of Slow Electrons in Solids

E. BAUER

Michelson Laboratory, China Lake, California 93555

Abstract

A theory of the inelastic scattering of slow electrons in solids due to excitation of interband transitions is developed. It is shown that both nondirect and direct transitions occur which can be described by a generalization of the formalism used in solid state optics. Experiments with 30-200 eV electrons scattered from Si(111) surfaces with well defined surface structures as determined by low energy electron diffraction confirm the theoretical predictions. They indicate that the inelastic scattering of slow electrons can be understood in terms of the three-dimensional band structure of solids and suggest the use of inelastic low energy electron scattering as a tool for band structure analysis.

I. Introduction

The inelastic scattering of medium fast electrons, i.e., electrons in the energy range from about 10^3 to 10^5 eV, in solids has been extensively studied during the past 20 years and appears to be reasonably well understood[1] in terms of the dielectric theory of solids[2]. In this theory the response of

---

[1] RAETHER, H.: Springer Tracts in Mod. Phys. 38, 84 (1965).

[2] ZIMAN, J.M.: Principles of the Theory of Solids, p. 126. Cambridge: University Press, 1964.

Encl (2)

the many-electron system of the solid to the disturbance introduced by the incident electron is described by the dielectric response function ("dielectric constant") $\varepsilon(\kappa,\omega)$, where κ and ω are the momentum and energy of the excitation produced by the incident electron. This $\varepsilon(\kappa,\omega)$ can be calculated from the energy band structure of the solid, which in turn is obtained from its potential. Unlike the elastic scattering, the inelastic scattering has not been directly related to the crystal potential, but in a rather indirect manner. The reason for this is two-fold: first, the direct relation between inelastic scattering and crystal potential is rather complex as will be seen in Section II; second, the function $\varepsilon(0,\omega)$ is known from optical measurements and describes surprisingly well the inelastic scattering of medium fast electrons[1]. This is due to the fact that the solid state excitations produced with significant probability have small momenta, e.g., long wavelength plasmons, or are connected with zero momentum change, e.g., direct interband transitions.

In the inelastic scattering of slow electrons, i.e., electrons with energies from several electron volts to several hundred electron volts, the approximation $\kappa \approx 0$ is inappropriate. Evidence for this is the observation that the inelastic scattering of slow electrons, similar to the elastic scattering of slow electrons, is less peaked in the forward direction than that of medium fast electrons[3,4]. The momentum κ of the excitation is equal to the momentum change $\Delta K = K' - K$ of the incident electron -- neglecting for

---

[3] MASSEY, H.S.W., and E.H.S. BURHOP: Electronic and Ionic Impact Phenomena, p. 93. Oxford: University Press, 1952.

[4] VAN VOORHIS, S.N.: Phys. Rev. 46, 480 (1934).

the moment the momentum $2\pi\vec{h}$ ($\vec{h}$ is a reciprocal lattice vector) transferred to the lattice and possible phonon contributions q. If significant scattering into relatively large angles, say $\theta = 20°$ occurs ($\theta = \sphericalangle(K,K')$) then $\kappa = K - K'$ is not negligible compared to the dimensions of the reciprocal lattice and the assumption $\kappa \approx 0$ is not valid: "nondirect" interband transitions ($\kappa \neq 0$) can be excited to a considerable extent in addition to the direct transitions so that $\varepsilon(0,\omega)$ becomes unsuited for the description of the inelastic scattering process. In spite of the lower forward scattering of slow electrons as compared with medium fast electrons, the fraction of the electrons which is scattered directly into angles larger than 30° is in general small. In most experimental arrangements -- as, for example, the one described in Section III -- usually only electrons scattered into angles larger than 90° can be observed. Consequently, a single inelastic scattering process is unlikely to produce an observable electron. Several scattering events are necessary to scatter a sufficient number of inelastic electrons into the backward direction, the simplest process being inelastic scattering followed by diffraction (elastic scattering) or visa versa (see Section II). Finally, slow electrons differ from medium fast electrons in that they interact not only via Coulomb forces but also by exchange forces which are a consequence of the Pauli principle, i.e., of the antisymmetry of the wave functions of the system solid plus interacting electron. These exchange interactions are negligible above energies of several hundred electron volts but become significant below about 100 eV. A proper theory of the inelastic scattering of slow electrons must, therefore, take into account (a) $\kappa \neq 0$, (b) diffraction and (c) exchange. In Section II such a theory will be

presented; Section III reports some preliminary results which support the suggestion that nondirect interband transitions are important in low energy electron scattering. Section IV gives a discussion of results and compares them with other observations. The scope of the paper is limited to single electron excitations; plasma excitations by slow electrons, which show some unexpected phenomena, will be dealt with elsewhere.

II. Theory*

The following basic assumptions are made:

(1) Only one "extra" electron is in the crystal at any time.

(2) The electron undergoes only one inelastic scattering process.

(3) The interaction between the electron and the crystal is described by the Schrödinger equation

$$H\Phi = E\Phi, \tag{1}$$

where

$$H = \sum_{j=1}^{N+1} \left[-\frac{1}{2}\nabla_{r_j}^2 - \sum_{k=1}^{N/\bar{Z}} \frac{Z_k}{|r_j - R_k|} + \sum_{k>j}^{N+1} \frac{1}{|r_j - r_k|} \right]$$

$$= \sum_j \left[-\frac{1}{2}\nabla_j^2 - \sum_k \frac{Z_k}{R_{jk}} + \sum_k \frac{1}{r_{jk}} \right] = \sum_j H(j). \tag{2}$$

The first term in the sum is the kinetic energy of the j-th electron, the second is its potential energy in the field of all nuclei -- $\bar{Z}$ is the average charge per nucleus -- and the third term is its potential energy in the field of all other electrons.

---

*Hartree atomic units are used throughout this paper.

(4) The total wave function of the system is given by

$$\Phi = \sum_{n=0}^{n_o} \Phi_n, \tag{3}$$

where the summation goes over all states n of the crystal and includes an integration over the continuum states and

$$\Phi_n = \frac{1}{\sqrt{(N+1)!}} \begin{vmatrix} \phi_n(1),\ldots, \phi_n(i-1), \phi_n(i), \phi_n(i+1),\ldots, \phi_n(N+1) \\ a_{n1}(1),\ldots,a_{n1}(i-1),a_{n1}(i),a_{n1}(i+1),\ldots,a_{n1}(N+1) \\ \ldots\ldots,\ldots,\ldots\ldots,\ldots\ldots,\ldots\ldots,\ldots,\ldots\ldots \\ a_{nN}(1),\ldots,a_{nN}(i-1),a_{rN}(i),a_{nN}(i+1),\ldots,a_{nN}(N+1) \end{vmatrix}$$

$$= -\frac{1}{\sqrt{N+1}} \sum_{i=1}^{N+1} (-1)^i \frac{1}{\sqrt{N!}} \begin{vmatrix} a_{n1}(1),\ldots,a_{n1}(i-1),a_{r1}(i+1),\ldots,a_{n1}(N+1) \\ \ldots\ldots,\ldots,\ldots\ldots,\ldots\ldots,\ldots,\ldots\ldots \\ a_{nN}(1),\ldots,a_{nN}(i-1),a_{rN}(i+1),\ldots,a_{nN}(N+1) \end{vmatrix} \phi_n(i)$$

$$= -\frac{1}{\sqrt{N+1}} \sum_{i=1}^{N+1} (-1)^i \psi_n(i^{-1}) \phi_n(i). \tag{4}$$

Here the ϕ_n and a_{nj} are the wave functions of the "extra" and of the "crystal" electrons, respectively, and the arguments i represent the space and spin coordinates r_i, σ_i.

(5) The "extra" electron has negligible influence on the wave functions of the "crystal" electrons. This implies that the wave functions are not localized in space, an assumption which is also made in the derivation of Koopman's theorem (see e.g., ref. 5).

Because of assumption (5) the $\psi_n(i^{-1})$ in Eq.(4) are solutions of the Schrödinger equation of the crystal without the extra electron (N electron system):

---

[5] SEITZ, F.: The Modern Theory of Solids, p. 313. New York: McGraw-Hill, 1940.

$$H(i^{-1})\psi_n(i^{-1}) = E_n\psi_n(i^{-1}), \tag{5}$$

where

$$H(i^{-1}) = H - H(i) = \sum_{\substack{j=1 \\ j\neq i}}^{N+1}\left[-\frac{1}{2}\nabla_j^2 - \sum_k \frac{Z_k}{R_{jk}} + \sum_{k>j}\frac{1}{r_{jk}}\right]. \tag{6}$$

The ψ_n are assumed to be orthonormal:

$$\int \psi_m^*(i^{-1})\psi_n(i^{-1})dx_i^{-1} = \delta_{mn}. \tag{7}$$

Here dx_i^{-1} denotes integration and summation over all space and spin coordinates respectively, except over r_i,σ_i. Because of the antisymmetry of the ψ_n (see Eq. (4)) the sum over i in Eq. (4) may be rewritten as

$$\Phi_n = \frac{1}{\sqrt{N+1}}\left[\psi_n(1^{-1})\phi_n(1) - N\,\psi_n(2^{-1})\phi_n(2)\right]. \tag{8}$$

The Schrödinger equations for the $\phi_n(1)$ can now be obtained by multiplying Eq. (1) with $\psi_m^*(1^{-1})$ $(m = 0,\ldots,n_o)$ and integrating over all coordinates except r_i,σ_i:

$$\int \psi_m^*(1^{-1})[H - E]\sum_{n=0}^{n_o}\Phi_n dx_1^{-1} = 0. \tag{9}$$

Use of Eqs. (2) and (5) - (8) leads to

$$\left[-\frac{1}{2}\nabla_1^2 - \sum\frac{Z_1}{R_{1k}} - (E - E_m)\right]\phi_m(1) + \sum_{n=0}^{n_o}\left[\int\psi_m^*(1^{-1})\sum_{k=2}^{N+1}\frac{1}{r_{1k}}\psi_n(1^{-1})dx_1^{-1}\phi_n(1)\right.$$
$$\left. - N\int\psi_m^*(1^{-1})[H - E]\psi_n(2^{-1})\phi_n(2)dx_1^{-1}\right] = 0. \tag{10}$$

With the definitions

$$K_m^2 = 2(E - E_m) \tag{11}$$

$$H_{mn}(1) = 2\int\psi_m^*(1^{-1})\sum_{k\geq 2}\frac{1}{r_{1k}}\psi_n(1^{-1})dx_1^{-1} \tag{12}$$

$$W_{mn}(1) = 2N \int \psi_m^*(1^{-1})[H - E]\psi_n(2^{-1})\phi_n(2)dx_1^{-1} \tag{13}$$

$$H'_{mm}(1) = -2 \sum_k \frac{Z_k}{R_{1k}} + H_{mm}(1), \tag{14}$$

Eq. (10) can be rewritten as

$$\left[\nabla_1^2 + K_m^2 - H'_{mm}(1)\right] \phi_m(1) + W_{mm}(1) = \sum_{n \neq m} \left[H_{mn}(1)\phi_n(1) - W_{mn}(1)\right] \tag{15}$$

$$m,n = 0,\ldots,n_o.$$

Here H'_{mm} is the potential energy of the "extra" electron in the field of the nuclei and electrons of the crystal; W_{mm} is the exchange term; the terms $H_{mn}\phi_n$ represent virtual and real electron-induced transitions (polarization and excitation) not involving exchange; and the $W_{mn}(n \neq m)$ are the corresponding terms involving exchange.

The integrals over the determinantal wave functions ψ (Eqs. (12),(13)) can be reduced to integrals over one-electron wave functions a,ϕ if it is assumed that these are mutually orthogonal. As shown in standard works -- see e.g., refs. 6,7 -- this leads to

$$H_{mm}(1) = 2 \sum_{i=1}^{N} \int a_{mi}^*(2) \frac{1}{r_{12}} a_{ni}(2)dx_2 \tag{16}$$

$$H_{mn}(1) = 2 \int a_{mi_o}^*(2) \frac{1}{r_{12}} a_{ni_o}(2)dx_2 \qquad (n \neq m). \tag{17}$$

In Eq. (17) a_{mi_o} and a_{ni_o} are the only wave functions which are different in the determinants ψ_m and ψ_n and are assumed to stand at the same places in these determinants. Integrals in which ψ_m differs from ψ_n in more than one wave function vanish.

---

[6] SLATER, J.C.: Quantum Theory of Atomic Structure, vol. I, p. 291. New York: McGraw-Hill, 1960.

[7] CONDON, E. U., and G. H. SHORTLEY: The Theory of Atomic Spectra, p. 169. Cambridge: University Press, 1953.

The corresponding one-electron expressions for $W_{mn}(1)$ are obtained if the "post interaction" form[8] of Eq. (13) is used

$$W_{mn}(1) = 2N \int \psi_m^*(1^{-1}) \left[-\frac{1}{2}\nabla_1^2 - \sum_k \frac{Z_k}{R_{1k}} - \frac{1}{2}K_m^2 + \sum_{k\geq 2} \frac{1}{r_{1k}} \right] \psi_n(2^{-1})\phi_n(2)dx_1^{-1}. \quad (13a)$$

This form follows from Eqs. (2), (5), (6) and from the hermitian property of the crystal hamiltonian $H(1^{-1})$:

$$\int \psi_m^*(1^{-1})H(1^{-1})\psi_n(2^{-1})\phi_n(2)dx_1^{-1} = \int \psi_n(2^{-1})\phi_n(2)H^*(1^{-1})\psi_m^*(1^{-1})dx_1^{-1}$$

$$= E_m \int \psi_n(2^{-1})\phi_n(2)\psi_m^*(1^{-1})dx_1^{-1} .$$

Expressing all ψ_m in terms of one-electron functions a_{mi}, using their orthogonality and imposing the orthogonality conditions

$$\int a_{mi}(1)\phi_n(1)dx_1 = 0 \qquad \text{for all } i,m,n \quad (18)$$

leads to the expressions

$$W_{mm}(1) = 2 \sum_{i=1}^{N} \int a_{mi}^*(2) \frac{1}{r_{12}} \phi_m(2)dx_2 \cdot a_{mi}(1) \quad (19)$$

$$W_{mn}(1) = 2 \int a_{mi_o}^*(2) \frac{1}{r_{12}} \phi_n(2)dx_2 \cdot a_{ni_o}(1). \quad (20)$$

In the derivation of Eq. (20) the same assumptions regarding the positions of the a_{mi} and a_{nk} which are different in the determinants ψ_m, ψ_n have been made. Omission of the orthogonality conditions (Eq. (18)) -- which have to be included in the Schrödinger equation with the help of Lagrangian multipliers -- leads to much more complicated expressions.

---

[8] SEATON, M.J.: Trans. Roy Soc. A245, 469 (1953).

Following SLATER[9], Eqs. (19) and (20) may be rewritten as

$$W_{mm}(1) = 2 \sum_i \int \frac{\phi_m^*(1) a_{mi}^*(2) \frac{1}{r_{12}} \phi_m(2) a_{mi}(1)}{\phi_m^*(1)\phi_m(1)} dx_2 \cdot \phi_m(1) = H_{mm}^{ex}(1) \cdot \phi_m(1) \quad (19a)$$

$$W_{mn}(1) = 2 \int \frac{\phi_n^*(1) a_{mi_o}^*(2) \frac{1}{r_{12}} \phi_n(2) a_{ni_o}(1)}{\phi_n^*(1)\phi_n(1)} dx_2 \cdot \phi_n(1) = H_{mn}^{ex}(1) \cdot \phi_n(1), \quad (20a)$$

where H_{mm}^{ex} and H_{mn}^{ex} may be considered as exchange potentials. It should be noted that the summation in Eqs. (19), (19a) is only over those "crystal" electrons whose spin is parallel to that of the "extra" electron because $\int \ldots dx_2$ includes also a summation over spin coordinates and because of the orthogonality of wave functions with opposite spin. For the same reason the summation in Eq. (16) is over all "crystal" electrons with parallel spin irrespective of the spin of the "extra" electron. This means that H_{mn} represents transitions between crystal states with the same spin, while H_{mn}^{ex} represents transitions between crystal states with opposite spins, the total spin of the system being conserved by spin exchange between "crystal" electron and the "extra" electron.

With Eqs. (16), (17), (19a), (20a), Eq. (15) may be written in the following way, assuming that condition Eq. (15) is fulfilled

$$\left[\nabla_1^2 + K_m^2 - (H'_{mm}(1) - H_{mm}^{ex}(1))\right] \phi_m(1) = \sum_{n \neq m}^{n_o} (H_{mn}(1) - H_{mn}^{ex}(1))\phi_n(1) \quad (21)$$

$$m,n = 0,\ldots,n_o \, .$$

In this form the equations describing the interaction of slow electrons with a crystal differ only in the exchange terms H_{mm}^{ex}, H_{mn}^{ex} from the corresponding

---

[9] SLATER, J.C.: Quantum Theory of Atomic Structure, vol. II, p. 7. New York: McGraw-Hill, 1960.

equations for medium fast electrons[10,11]. In the theory for medium fast electrons the following assumptions are made: (1) all $H_{mn} \ll H_{oo}$ $(m \neq n,o)$ and (2) all $\phi_n \ll \phi_o$, i.e., the "inelastic wave field" ϕ_n in the crystal resulting from the excitation of the state n of the crystal by the "elastic wave field" ϕ_o is small compared to ϕ_o. The elastic wave field ϕ_o consists of the incident and all elastically scattered waves. For slow electrons the additional assumption (3) must be made that all $H^{ex}_{mn} \ll H^{ex}_{oo}$ $(m \neq n,o)$. Assumptions (1) and (3) imply that the inelastic waves are coupled with the elastic wave field but not with each other and that they are subject to diffraction. Then the Eqs. (21) for the elastic and inelastic wave fields in the crystal simplify to

$$\left[\nabla^2 + K_o^2 - H^T_{oo}\right]\phi_o = \sum_{n=1}^{n_o} H^T_{on}\phi_n \tag{22}$$

$$\left[\nabla^2 + K_m^2 - H^T_{mm}\right]\phi_m = H^T_{mo}\phi_o \qquad m = 1,\ldots,n_o \ , \tag{23}$$

where

$$H^T_{mm} = H'_{mm} - H^{ex}_{mm} \tag{24}$$

and

$$H^T_{mn} = H_{mn} - H^{ex}_{mn} \ . \tag{25}$$

The formal solution of Eq. (23) which has the proper asymptotic form is given by[12]

$$\phi_m(r) = \int G^+_n(r,r')\ H^T_{mo}(r')\phi_o(r')dr' \ , \tag{26}$$

---

[10] YOSHIOKA, H.: J. Phys. Soc. Japan 12, 618 (1957).

[11] RADI, G.: Z. Phys. 212, 146 (1968).

[12] MOTT, N.F., and H.S.W. MASSEY: The Theory of Atomic Collisions, 3rd ed., p. 69. Oxford: University Press, 1965.

where the outgoing Green's function $G_m^+(r,r')$ is the solution of

$$\left[\nabla^2 + K_m^2 - H_{mm}^T\right] G_m^+(r,r') = \delta(r - r'). \tag{27}$$

The physical meaning of Eq. (26) is very simple: each volume element dr' of the crystal emits an inelastic wavelet $\delta\phi_m(r')$ whose amplitude is proportional to the amplitude $\phi_o(r')$ of the elastic wave field and to the probability $H_{mo}^T(r')$ of the excitation which produces the inelastic wavelet. The Green's function $G_m^+(r,r')$ describes the propagation of the wavelet $\delta\phi_m(r')$ from r' to r which involves -- for $H_{mm}^T \neq 0$ -- diffraction by the (excited) crystal. If diffraction of $\delta\phi_m(r')$ is neglected, i.e., if $H_{mm}^T = 0$, $G_m^+(r,r')$ is given by[12]

$$G_m^+(r,r') = -\frac{1}{4\pi}\frac{e^{iK_m|r-r'|}}{|r-r'|} \to -\frac{1}{4\pi}\frac{e^{iK_m r}}{r} e^{-iK_m \cdot r'} \qquad \text{for } |r| >> |r'| ,$$

where $K_m = nK_m$ and n is the unit vector in direction r. Consequently,

$$\phi_m(r) \to -\frac{1}{4\pi}\frac{e^{iK_m r}}{r}\int e^{-iK_m \cdot r} H_{mo}^T(r')\phi_o(r')dr' . \tag{28}$$

Obviously this neglection is not permissible because, by the same token, the diffraction of the incident wave would have to be neglected too, so that $\phi_o(r') = e^{iK_o r'}$ (first Born approximation).

Therefore, the diffraction of both the elastic and inelastic waves in the crystal has to be taken into account simultaneously, i.e., Eqs. (27) and the integro-differential equation obtained by introducing Eq. (26) into Eq. (22) must be solved. While the solution of this problem for medium fast electrons has made considerable progress[11], its solution for slow electrons is still in its very early stages. Therefore, no more explicit, meaningful expressions for ϕ_m can be given at present. However, some general conclusions

regarding ϕ_m may be drawn from Eq. (26) using some general aspects of the diffraction process, and of the form of H_{mo}^{T} as expressed in terms of crystal wave functions.

In most inelastic electron scattering experiments only the asymptotic form of ϕ_m is needed (r is outside of the crystal and $|r| >> |r'|$). In this case $G_m^+(r,r')$ may be written in the form[12]

$$G_{m,as}^{+}(r,r') = \frac{e^{iK_m r}}{r} F_m(r') \ . \tag{29}$$

With Kainuma's[13] implicit approximation $F_m(r') = \phi_m(r')$, the validity range of which needs examination, and with Eqs. (17), (20a) and (25), the asymptotic form of ϕ_m Eq. (26) may be written as

$$\phi_{m,as}(r) = \frac{e^{iK_m r}}{r}\left[2\int \phi_m(r')a_m(r'') \frac{1}{|r'-r''|} a_o(r'')\phi_o(r')dr'dr'' + E.T. \right]$$

$$= \frac{e^{iK_m r}}{r} f_m \ , \tag{30}$$

where E.T. represents the exchange term resulting from the contribution of H_{mo}^{ex} to H_{mo}^{T} (Eq. (20a)) and the subscript i_o in a_{mi_o} and a_{ni_o} has been dropped.

The scatterer in most low energy electron scattering experiments is a flat single crystal surface which can be approximated by a periodic half space. The one-electron wave functions in such a system are two-dimensional Bloch functions. If the scattering data are to be compared with the (three-dimensional) band structure of the crystal, i.e., if three-dimensional Bloch functions $a_m(k',r''),a_o(k,r'')$ are assumed for a_m,a_o, then consistency requires that the same be done for ϕ_m and ϕ_o. The validity of this assumption will be examined experimentally in Part III.

---

[13] KAINUMA, Y.: Acta Cryst. 8, 247 (1955).

The detector in most scattering experiments measures the electron current regardless of electron spin. The current density j_m in the spherical wave given by Eq. (30) is

$$j_m = \frac{1}{2i}\left[\phi^*_{m,as}\nabla\phi_{m,as} - \phi_{m,as}\nabla\phi^*_{m,as}\right] = \frac{K_m}{r^2}|f_m|^2\frac{r}{r} . \tag{31}$$

The current across the surface element $r^2 d\Omega$ of a sphere with radius r, i.e., the current scattered into the solid angle $d\Omega$ and normalized to unit current in the incident beam, is then

$$\frac{j_m}{j_o} d\Omega = \frac{K_m}{K_o}|f_m|^2 d\Omega . \tag{32}$$

The detector is usually some sort of electron energy analyzer which allows one to measure the energy difference ΔE between the electron energy before and after the inelastic scattering process. The energy ΔE is transferred to the crystal electron in the transition from its ground state with energy $E_o(k)$ to the excited state with energy $E_m(k') = E_o(k) + \Delta E$. In the energy band structure of a crystal (see Fig. 1)[14] there is a finite or infinite number of k,k' pairs -- depending upon the restrictions imposed on $k' - k = \Delta k$ -- for which

$$E_m(k') - E_o(k) = \Delta E . \tag{33}$$

Furthermore, each state consists of several bands characterized by the indices μ,ν. For example, the ground state 0 (valence band) and excited state m (conduction band) of the four valence electrons of silicon consist of four bands $(0,\nu)$ and (m,μ) respectively ($\mu,\nu = 1 \ldots 4$). At symmetry points (e.g., at Γ) and along certain symmetry directions (e.g., along Λ) these bands are partially degenerate, but at general points in the Brillouin zone and along Σ they are

nondegenerate (see Fig. 1)[14]. The existence of several bands in each state increases the number of k,k' pairs for which Eq. (33) is fulfilled.

There are, therefore, many possibilities for an electron to lose the energy ΔE which can be taken into account by a k-integration over the Brillouin zone and by summing (or integrating) over all allowed Δk for which Eq. (33) is fulfilled:

$$I(\Delta E) = \sum_{\mu,\nu} \sum_{\Delta k_i} \int \frac{j_{m\mu\nu}(k,k+\Delta k_i)}{j_o} \delta(E_{m\mu}(k+\Delta k) - E_{o\nu}(k) - \Delta E)dk \ . \qquad (34)$$

The δ function has the property[15]

$$\int g(k)\delta[f(k)]dk = \int g(k) \ |\nabla_k(f(k)|^{-1}_{k=k_o} \ d^2k \qquad \text{with } f(k_o) = 0, \qquad (35)$$

where d^2k is a surface element in k space on the surface defined by $f(k) = 0$. Applying Eq. (35) to Eq. (34) leads to

$$I(\Delta E) = \sum_{\mu,\nu} \sum_{\Delta k_i} \int \frac{j_{m\mu\nu}(k,k+\Delta k_i)}{j_o} \frac{1}{|\nabla_k(E_{m\mu}(k,k+\Delta k_i)-E_{o\nu}(k))|} d^2k \qquad (34a)$$
$$E_{m\mu}-E_{o\nu}=\Delta E$$

The second term in the integral goes towards infinity for $k,\Delta k_i$ pairs $(k_o,\Delta k_i)$ for which

$$\nabla_k(E_{m\mu}(k_o,k_o + \Delta k_i)) = \nabla_k E_{o\nu}(k_o) \ , \qquad (36)$$

i.e., for $k,\Delta k_i$ pairs for which the energy bands of the ground state and the excited state are parallel. If it is assumed -- as it is done similarly in optical reflectivity of solids -- that $j_{m\mu\nu}(k,k+ k_i)$ varies slowly with k on the surface of integration near $k_o,\Delta k_i$ then $j_{m\mu\nu}$ may be removed from the

---

[14] HERMAN, F., R. L. KORTUM, and C.D. KUGLIN: Internat. J. Quantum Chem. 1s, 533 (1967).

integral and replaced by its value at $k_o, \Delta k_i$. If the additional assumption is made that $j_{m\mu\nu}$ is not very small at $k_o, \Delta k_i$, as compared to its value for $k, \Delta k_i$ pairs for which the second term is small, then all contributions to the integral in Eq. (34) other than those from $k_o, \Delta k_i$ may be neglected and Eq. (34) may be written as

$$I(\Delta E) = \sum_{\mu,\nu} \sum_{\Delta k_i} \frac{j_{m\mu\nu}(k_o, \Delta k_i)}{j_o} J_{mo\mu\nu}(\Delta E, \Delta k_i) , \tag{37}$$

where

$$J_{mo\mu\nu}(\Delta E, \Delta k_i) = \int \frac{d^2k}{|\nabla_k (E_{m\mu}(k, k+\Delta k_i) - E_{o\nu}(k))|} \quad E_{m\mu} - E_{o\nu} = \Delta E \tag{38}$$

Equation (38) is a generalization of the joint density-of-states function widely used in the analysis of optical reflection spectra of solids[15] which is obtained for $\Delta k_i = 0$. Therefore, it will be called generalized joint density-of-states function. Point pairs $k, k_i' = k+\Delta k_i$ in reciprocal space for which Eq. (36) is fulfilled will be called critical point pairs in analogy to the critical points ($\Delta k_i = 0$) known from optics[15].

Equations (37) and (38) show that $I(\Delta E)$ will have maxima as function of ΔE whenever condition (36) is fulfilled for one or several $k, k+\Delta k_i$ pairs. The heights and widths of these maxima depend, among other factors, upon: (1) The height and width of $J_{mo\mu\nu}(\Delta E)$ for a given Δk_i; (2) The number of allowed Δk_i to be considered for a given ΔE; and (3) The contributions from multiple and from phonon-assisted inelastic scattering which are not included in the present theory.

---

[15] BASSANI, G.F.: in The Optical Properties of Solids, ed. by J. Tauc, p. 33. New York: Academic Press, 1966.

Factor (3) will certainly introduce a ΔE-dependent background, but its significance is difficult to assess at the present time for lack of sufficient experimental data. An estimate of the influence of factor (1) can be obtained from KANE'S calculations[16] of $\varepsilon_2(0,\omega)$ for silicon. $\varepsilon_2(0,\omega)$ is given by an expression similar to Eqs. (34) and (34a) with $\Delta k_i = 0$ and $\frac{j_{m\mu\nu}}{j_o}$ replaced by the momentum matrix element between ground and excited states. Kane found that large fractions of the Brillouin zone contribute to $\varepsilon_2(0,\omega)$ for all ω, and that the maxima in $\varepsilon_2(0,\omega)$ are only in part due to critical points. Therefore, even when only one Δk_i has to be considered, the maxima in $I(\Delta E)$ will be much less pronounced than one could expect from Eqs. (37) and (38). The maxima will be even less pronounced when several Δk_i have to be taken into account. The need for taking at least several Δk_i into account in electron scattering experiments can be seen upon closer inspection of Eq. (30), for example, by approximating all wave functions in Eq. (30) by plane wave expansions. Then the integral in Eq. (30) splits up into linear combinations of integrals of the form

$$\int e^{-iK^{\alpha}_{mh_i} r'} \, e^{-ik^{\beta}_{mh_k} r''} \, \frac{1}{|r'-r''|} \, e^{ik^{\gamma}_{oh_\ell} r''} \, e^{iK^{\delta}_{oh_p} r'} \, dr'dr'' + \text{E.T.} \qquad (39)$$

with r', r'' independent coefficients. Equation (30) and, therefore, the integrals Eq. (33) have to be invariant against lattice translations $a = n_1a_1 + n_2a_2 + n_3a_3$ where n_1, n_2, n_3 are integers and a_1, a_2, a_3 are the unit cell dimensions of the crystal. This invariance requires that

$$e^{i\left[-K^{\alpha}_{mh_i} - k^{\beta}_{mh_k} + k^{\gamma}_{oh_\ell} + K^{\delta}_{oh_p}\right] \cdot a} = 1$$

---

[16] KANE, E.O.: Phys. Rev. 146, 558 (1966).

for all $\alpha,\beta,\gamma,\delta,i,k,\ell,p$, a condition which is fulfilled only if the parentheses in the exponent equals $2\pi h$, where h is a reciprocal lattice vector. Because by definition $K_h = K + 2\pi h$, $k_h = k + 2\pi h$, and because the sum of several reciprocal lattice vectors is again a reciprocal lattice vector, the translational invariance requirement leads to the momentum conservation law

$$\Delta k = k_m^\beta - k_o^\gamma = K_o^\delta - K_m^\alpha + 2\pi h. \tag{40}$$

The superscripts refer to all the waves within the crystal which have the same tangential components as the corresponding waves K_o, K_m outside the crystal. The right side of Eq. (34) can also be written in the form $K_o^\delta + 2\pi h' - (K_m^o + 2\pi h'')$ and interpreted as follows: the incident wave with wave vector K_o produces by diffraction a wave field of elastic waves with wave vectors $K_o^\delta + 2\pi h'$ in the crystal. Each of these waves contributes by excitation of the crystal to the inelastic wave field with wave vectors $K_m^\alpha + 2\pi h''$ in the crystal. These conclusions are valid also for other approximations in which the "extra" and the "crystal" electrons are described by wave functions not localized in space.

An energy analyzer of such high angular resolution that it collects only electrons scattered in the direction of K_m detects, therefore, not only those electrons with energy loss ΔE which have been produced by the incident wave, but also all those produced by diffraction into direction K_m either before or after the energy loss. Ordinarily, only a limited number of waves have to be considered, namely those for which the Bragg condition $\Delta K = 2\pi h$ is approximately fulfilled. Under favorable conditions only two or three strong waves exist in the crystal. In this case the directions of K_m and the values

of ΔE for which the scattered current has maxima can -- on the basis of Eqs. (33), (34a) and (36) -- give information on the energy band structure of the crystal which cannot be obtained from optical measurements where $\Delta k = 0$.

An energy analyzer which integrates over a large solid angle range like the one described in Section III detects electrons scattered in all directions K_m within this solid angle. Therefore, even if only a small number of diffracted waves has to be considered, Δk becomes a continuous variable and the summation over Δk_i in Eq. (34a) has to be replaced by an integration. This will tend to smear out the structure in $I(\Delta E)$ and eliminate the possibility of associating ΔE values for which $I(\Delta E)$ has maxima with k,k' pairs for which the bands are parallel. Nevertheless, some structure in $I(\Delta E)$ is to be expected; it could be especially pronounced for special K_o which lead to favorable diffraction and excitation conditions. This will be examined experimentally in Section III.

In concluding the theoretical considerations it should be pointed out that they are largely based on the three-dimensional periodicity of the crystal. The wave functions near a plane crystal surface have, however, only two-dimensional periodicity, i.e., are two-dimensional Bloch functions. The solution of the elastic scattering problem alone, neglecting inelastic scattering completely, (all $\phi_m = 0$ except ϕ_o) is in such an early stage[17] that the discussion of the combined problem appears premature. However, it is well known from experiment that the three-dimensional diffraction conditions are considerably relaxed, thus leading to a further smearing out of the structure in $I(\Delta E)$.

---

[17] KAMBE, K.: Z. Naturforschg. 22a, 322, 422 (1967); 23a, 1280 (1968).

III. Experiment

The goal of the experiment is to determine whether or not an interpretation of the energy loss spectrum $I(\Delta E)$ of slow electrons in solids in terms of the three-dimensional band structure is justified. This can be done by measuring $I(\Delta E)$ for a surface which can exist in several structures. If $I(\Delta E)$ does not change significantly with the surface structure -- some change is to be expected because of the differences in the diffraction process between the various structures -- and if the ΔE values for which $I(\Delta E)$ has maxima can be related to interband transitions, then the three-dimensional treatment appears permitted. The silicon (111) surface is singularly suited for this purpose. It is known to exhibit several surface structures which can be produced easily, and the band structure of silicon has been extensively studied.

The experimental setup should (1) allow monitoring of the surface structure, (2) integrate over a sufficiently large solid angle to minimize the differences due to diffraction effects, (3) be sensitive to weak structure in $I(\Delta E)$, and (4) have high energy resolution. Conditions (1) to (3) are fulfilled in the experimental setup first described by WEBER and PERIA[18], which combines display-type low energy electron diffraction (LEED) with the measurement of $I(E)$ and $\frac{dI(E)}{dE}$. High energy resolution (condition (4)) can be achieved by the following modifications of the Varian three-grid LEED system (see Fig. 2): (1) Connection of grid 3 with grid 2. This provides a better defined filter potential; (2) Compensation of the capacitive current between grid 3 and the collector. This is achieved by putting the capacitance between grid 3 and collector in one arm of a capacitance bridge and an adjustable capacitor into the other arm and balancing

[18] WEBER, E.E., and W.T. PERIA: J. Appl. Phys. 38, 4355 (1967).

the bridge with zero electron current in the most sensitive range of the lock-in amplifier; (3) Use of lower filter-voltage-modulation amplitudes than those used generally. In order to obtain a sufficiently large reference amplitude for the lock-in amplifier (PAR 121) an A.C. amplifier between oscillator and reference input is necessary.

Figure 3 shows the dependence of the "inflection width" W_I of the peak of the elastically reflected electrons upon modulation voltage V_M (peak to peak). W_I is defined by the distance between maximum and minimum in $\frac{dI}{dE}$, i.e., by the distance between the points of maximum slope of I(E). $W_I(V_M)$ is independent of primary energy E in the range studied (30 eV < E < 200 eV). The modulation voltage suggested by Fig. 3 is 1.2 V*, Figure 4 shows a typical energy distribution I*(ΔE) (a) and its derivative (b) for 50 eV electrons normally incident onto a Si(111) surface with well pronounced 7x7 structure (see below). The advantage of measuring the derivative of I* for detecting weak structure in I*(ΔE) is obvious. It should be noted, that I*(ΔE) is not identical with the I(ΔE) of Eqs. (34), (34a) and (37), but is obtained from it by integrating over all K_m directions intercepted by the collector and by folding with an apparatus function which contains parameters such as the energy resolution of the grid system, the energy spread of the electron source and the modulation amplitude.

With this experimental setup and primary electron energies from 30 to 200 eV the following Si(111) surface structures were studied for various angles of incidence:

---

* If resolution is not the important quantity, higher modulation amplitudes -- from V_M = 1.4 V p.t.p. at E = 30 eV to V_M = 2.8 V p.t.p. at E = 200 eV -- give maximum A_I/W_I ratios.

1) 1x1 structure (Fig. 5a)

2) 7x7 structure (Fig. 5b)

3) $\sqrt{19}$ x $\sqrt{19}$ R(23.5°) structure (Fig. 5c)

The first structure may be obtained by annealing a slightly nickel-doped crystal for several minutes at 700°C to 800°C, preceded by heating to 1200-1300°C. The periodicity is that expected from the bulk lattice periodicity. The LEED pattern shows usually some weak diffuse background indicating very weak, poorly pronounced structure 3). The 7x7 structure is obtained by annealing a "clean" surface at 700°C to 800°C. It has been ascribed to a rearranged clean surface[19-22] or to a very thin silicide surface layer with the unit cell dimensions of Fe_5Si_3[23]. The third structure is obtained in nickel-containing samples by quenching from 900°C or higher. It has been attributed to the rearranged clean surface[19-22], to a rearranged surface stabilized by traces of nickel[24] and to a thin surface layer of a nickel-containing silicide[23]. The following results were obtained for these structures:

1. At the higher primary beam energies E there is little structure in the energy distribution derivative (E.D.D.) below $\Delta E = 10$ eV. Figure 6 illustrates this for E = 150 eV. There is only one "peak", the position of which shifts somewhat towards lower energies (4.6 → 4.5 → 4.2 eV) with decreasing amplitude

---

[19] SCHLIER, R.E., and H.E. FARNSWORTH: J. Chem. Phys. 30, 917 (1959).

[20] LANDER, J.J., and J. MORRISON: J. Chem. Phys. 37, 729 (1962); J. Appl. Phys. 34, 1403 (1963).

[21] SEIWATZ, R.: Surface Sci. 2, 473 (1964).

[22] HANSEN, N.R., and D. HANEMAN: Surface Sci. 2, 566 (1964).

[23] BAUER, E.: a) Phys. Letters 26, 530 (1963); b) in The Structure and Chemistry of Solid Surfaces, ed. by G.A. Somorjai. New York: John Wiley, in print.

[24] VAN BOMMEL, A.J., and F. MEYER: Surface Sci. 8, 467 (1967).

going from c to a to b. This and the following results suggest that this peak consists of two or more unresolved peaks, and that a decrease of the higher peaks causes the shift towards lower energies. The dominating feature in all cases is the volume plasmon peak which occurs in a and c at 18.2 eV, in b at 17.8 eV. The second feature which can be ascribed to plasmons occurs in a,b,c at 11.0, 11.2 and 12.0 eV, respectively; it increases considerably with angle of incidence and is, therefore, attributed to the surface plasmon peak. Between these two features is another one which is best pronounced in c and corresponds to a peak at 15.2 eV. While the volume (surface) plasmon peaks decrease (increase) considerably with angle of incidence, the 15.2 eV peak remains essentially unchanged.

2. With decreasing primary beam energy the low energy part of the E.D.D. becomes more and more structured. This is illustrated in Fig. 7 for E = 100 eV. The single low voltage peak at high E resolves into two peaks which are located at roughly 3.0 and 5.0 eV in all three surface structures of Fig. 7. In addition to the peaks at 11-12, 15.2 and about 18 eV mentioned above, an additional peak appears in Fig. 7 at 8.3 eV (in a) or 8.6 eV (in b,c). In contrast to the 11-12 eV peaks the 3.0, 5.0 and 8.3-8.6 eV peaks do not increase with angle of incidence.

3. At the lowest primary beam energies (30-40 eV) high resolution measurements are hampered by noise. Above E = 40 eV, however, considerable structure in the E.D.D. can be observed reproducibly. The peaks vary little in energy position ΔE but considerably in amplitude with E, the angles of incidence (θ,ϕ) and the surface structure. Rather than shifting in ΔE, peaks usually diminish and are partially or completely replaced by other peaks. An

E.D.D. selected for its pronounced structure is shown in Fig. 8. The $\Delta\tilde{E}$' values of the peaks (2.3, 5.2, 8.6, 11.2, 15.1, 17.6 eV) are the ones more frequently found in the low energy range. Other peaks occur at 3.3, 4.2, 7.5 eV.

4. The 15.2 eV peak frequently shows up only as a change in slope on the low ΔE side of the volume plasmon peak. In spite of this the amplitudes A_{vp} and $A_{15.2}$ (see Fig. 8) can be measured well enough to determine that the peaks differ in their energy dependence as shown schematically in Fig. 9. The experimental points scatter systematically suggesting a somewhat more complicated energy dependence. Figure 9 gives only the averaged shape of the curves.

IV. Discussion

To determine the origin of the energy losses observed at lower voltages the data can be compared either directly with the band structure[14] (Fig. 1) or with the dielectric function derived from optical reflectivity measurements (Fig. 10)[25]. Strong structure in $\varepsilon_2(\omega)$ or $\omega^2\varepsilon_2(\omega)$ is usually attributed to direct transitions, weak structure to indirect transitions. The main peaks at 3.45, 4.25 and 5.3 eV have been attributed to the direct transitions $\Gamma'_{25} \rightarrow \Gamma'_2$, $X_4 \rightarrow X_1$ and $L'_3 \rightarrow L_3$ (see, however, ref.16); the peaks at 1.6, 2.3 and 8.7 eV are probably due to indirect transitions. The origin of the structure at higher voltages (11.5, 14, 15.5, 17.5 eV) is not clear at present. The comparison between the E.D.D. curves and $\varepsilon_2(\omega)$ shows that all $I^*(\Delta E)$ peaks, except for the 7.5 eV peak, coincide within the error and fluctuation limits

---

[25] EDEN, R.C.: Stanford University Rep. No. SU-SEL-67-038 (1967), p. 297.

with peaks in $\varepsilon_2(\omega)$ or $\omega^2\varepsilon_2(\omega)$. This agreement strongly suggests an interpretation of the energy loss spectrum in terms of nondirect and direct interband transitions in the three-dimensional band structure -- except for the 11-12 and 13 eV peaks which are attributed to surface and volume plasmons, respectively. Direct transitions ($\Delta k = 0$) are possible whenever $K_m - K_o = 2\pi h$ (see Eq. (40)). Further support for the three-dimensional origin of the low lying loss peaks is the insensitivity of their position towards changes of the surface structure. The fact that their intensity does not increase with angle of incidence also speaks against a surface origin. Without the knowledge of the Δk associated with a given ΔE the transition involved can only be guessed. Two such guesses (2.3 and 8.6 eV) are indicated in Fig. 1.

The large number of transitions indicated in the E.D.D. curves at low E makes the loss of structure in the E.D.D. at higher voltages (Figs. 6,7) understandable. If, for example, the 2.3, 3.3, 4.2 and 5.2 eV losses occur simultaneously their overlap can easily wipe out all structure in this energy range. Other causes which are likely to have a similar effect are (1) multiple energy losses which increase the number of ΔE values and (2) phonon-assisted energy losses which increase the number of Δk's by addition of the phonon momentum. Another possible cause, however, can be excluded, namely, the increase of the number of $\Delta k = K_m - K_o - 2\pi h$ due to the increase of the number of propagating waves with voltage as evidenced by the number of diffraction spots h. This follows from three considerations: (1) Surfaces with completely different diffraction patterns, such as those shown in Fig. 5a and 5c, give essentially identical E.D.D. for $\Delta E \lesssim 10$ eV (see Fig. 6a and 6c). (2) Although at lower voltage the number of propagating waves h is smaller, the three-dimensional

diffraction conditions are relaxed considerably because there is a wider range of the normal components h_n of $h = h_t + h_n$ within which diffraction can occur, and, therefore, a wide range of possible Δk. (3) With increasing energy the inelastic scattering becomes increasingly peaked in the forward direction, thus reducing the probability of nondirect transitions (see e.g., Fig. 9). A compensation of this effect by the increase in phonon-assisted (indirect) transitions appears unlikely in the energy range studied because of the high spot to background intensity ratio in the LEED pattern.

The low energy E.D.D. results reported in Part III can also be compared with the energy loss spectra obtained with medium fast (50 keV) electrons. The volume and surface plasma losses for medium fast electrons are reported to occur at 16.9 and 10 eV, respectively[1]. These values are compatible with the values 17.3 (18.2) and 11-12 eV reported here if the dispersion of the energy losses is taken into account: the lower values are measured for zero scattering angle where the losses have their lowest value, while the higher values are obtained by integration over a wide scattering angle. In addition to the plasma losses, losses due to intraband transitions at 2.4, 3.2 and 5.3 eV have been reported[27], which agree well with the data given in Part III. The 3.2 and 5.3 eV peaks can be attributed to direct transitions (see above). The 2.4 eV peak has been explained in terms of retardation effects[28] which are connected with a high value of ε_1. Although the theory of this effect[29] predicts a thickness dependence of the retardation effects, the 2.4 eV peak could also be due to indirect

---

[27] ZEPPENFELD, K., and H. RAETHER: Z. Phys. 193, 471 (1966).

[28] FESTENBERG, C.V., and E. KRÖGER: Phys. Letters A26, 339 (1968).

[29] KRÖGER, E.: Z. Phys. 216, 115 (1968).

transitions. The probability for the excitation of indirect transitions (involving phonons) by medium fast electrons increases with film thickness. The mean free path for electron-phonon scattering of 50 keV electrons in Si at room temperature is about 5000 Å[30]. Therefore, a film thickness of several thousand angstroms is required before the momentum required in the indirect transition can be supplied with sufficient probability by a phonon. A study of the temperature dependence of this peak should allow clarification of this problem.

Finally, the data for Si may be compared with other recent low energy electron loss measurements. THARP and SCHEIBNER[31] who did the first systematic measurements of this kind on surfaces defined by LEED could not find any energy losses due to the excitation of interband transitions below 30 eV. JORDAN and SCHEIBNER[32] who studied Cu(100) and (110) surfaces attributed two of their losses (4.5 and 27.5 eV) to (direct) interband transitions, while the rest was assigned to plasma losses. In both metals the identification of the various energy losses with specific loss mechanisms is difficult. Thus, the 7.5 eV peak in Cu has been attributed to volume plasmon excitation[1] on the basis of optical measurements and to surface plasmon excitation[32]. This latter assignment is based on the criterion that if the height of a certain loss peak is sensitive to surface condition, e.g., oxygen adsorption, then this peak is due to surface plasmon excitation. (In W the loss peak attributed to the surface plasmon loss increases[31] with oxygen coverage, in Cu it decreases[32].)

---

[30] MEYER, G.: Phys. Letters 20, 240 (1966); Z. Naturforschg. 21a, 1524 (1966).

[31] THARP, L.N., and E.J. SCHEIBNER: Surface Sci. 8, 247 (1967); J. Appl. Phys. 38, 3320 (1967).

[32] JORDAN, L.K., and E.J. SCHEIBNER: Surface Sci. 10, 373 (1968).

The theoretical considerations of Part II and the experimental results of Part III show, however, that such a criterion is not reliable. A change in the surface condition which causes changes in the diffraction conditions as evidenced by the LEED pattern modifies the elastic and inelastic wave fields in the crystal, and thereby the excitation conditions which effects the probability of interband transitions and the height of the loss peaks associated with them. Thus, a distinction between surface plasmon and interband transition excitation on the basis of this criterion is difficult. A more reliable method for distinguishing between surface and volume effects is the study of the dependence of the peak heights upon angle of incidence of the primary beam as it was done in Part III. Simply for geometrical reasons the relative importance of surface effects has to increase with angle of incidence. Preliminary measurements[33] of this kind on a W(110) surface with 60-140 eV primary electrons do not show the expected angle of incidence dependence of the relative intensities of the loss peaks previously[11] attributed to volume and surface plasmon excitation. Therefore it is unlikely that the inelastic diffraction effects observed by Porteus[34] on the W(110) surface are connected with plasmons as suggested in ref. 31; they could equally well be considered as demonstration of the diffraction effects predicted in Part II.

---

[33] BAUER, E.: unpublished.

[34] PORTEUS, J. O.: in The Structure and Chemistry of Solid Surfaces, ed. by G. A. Somorjai. New York: John Wiley, in print.

The difficulty of distinguishing between volume plasmon, surface plasmon and interband transitions which occurs in metals like Cu and W can be avoided if metals are chosen in which the energies of volume and surface plasmon are well known because of their free electron gas-like behavior, e.g., Al, Mg, Be or the alkali metals[1]. Preliminary work[3] with thick (111) oriented epitaxial Al films on a Si(111) surface shows, in addition to the well defined surface and volume plasmon loss peaks, considerable structure in the E.D.C. below $\Delta E = 10$ eV. One of the peaks -- at about 1.8 eV -- can possibly be associated with the direct interband transition which produces an $\varepsilon_2(\omega)$ peak at 1.5 eV[1]. The remaining structure between 2 and 10 eV is probably due to nondirect transitions.

V. Conclusions

1. Theory predicts that nondirect transitions are the rule and not the exception in the inelastic scattering of slow electrons in contrast to optical reflectivity and inelastic scattering experiments with medium fast electrons.
2. The influence of the band structure on the energy loss distribution can be described by a generalization of the formalism used in the discussion of the optical absorption of solids.
3. Elastic and inelastic scattering are intimately coupled, complicating the interpretation of the energy loss spectra in terms of the band structure.
4. Experiment shows that in spite of this complication loss spectra integrated over a large scattering angle range exhibit structure which can be related to indirect and direct transitions.
5. The pronounced structure in the energy loss spectra for $\Delta E < 10$ eV which is observed for specific primary beam energies and angles of incidence makes it appear promising to study both energy and angular distribution of slow inelastically scattered electrons. This should give information on the energy band structure of solids ($\Delta E, \Delta k$ pairs) which cannot be obtained with other methods.
6. The position of the loss peaks is not much influenced by the surface structure of the crystal. This shows: (1) the surface layer contributes little to the inelastic scattering which is mainly determined by the three-dimensional band structure; (2) the mean free path for inelastic scattering is longer than that for elastic scattering in agreement with the theoretical predictions of ref. 23b.

The author wishes to thank Dr. V. Rehn and Dr. J. O. Porteus for stimulating discussions and for critically reading the manuscript. This work was sponsored by the National Aeronautics and Space Administration under Grant Number R-05-030-001.

Dr. E. Bauer
Code 6017
Michelson Laboratory
China Lake,
California 93555

FIGURE CAPTIONS

Fig. 1. Energy band structure of silicon[14]. Solid arrows indicate observed direct transitions, dashed arrows possible nondirect transitions (2.3 and 8.6 eV).

Fig. 2. Experimental setup for high resolution energy analysis.

Fig. 3. Dependence of energy resolution upon modulation amplitude.

Fig. 4. Energy loss spectrum and its derivative for 50 eV primary electrons from silicon (111) surface with 7x7 structure. Polar angle of incidence $\theta = 12°$ in $\langle 1\bar{1}0 \rangle$ azimuth. Numbers indicate lock-in amplifier sensitivity in mV.

Fig. 5. Low energy electron diffraction patterns of surface structures on the Si(111) plane with (a) 1x1, (b) 7x7 and (c) $\sqrt{19}$ x $\sqrt{19}$ R(23.5°) structure; taken with 40 eV primary electrons.

Fig. 6. Energy loss spectrum derivatives for 150 eV primary electrons from silicon (111) surfaces with the structures shown in Fig. 5a-5c. Angle of incidence as in Fig. 4.

Fig. 7. Energy loss spectrum derivatives for 100 eV primary electrons from silicon (111) surfaces with the structures shown in Fig. 5a-5c. Angle of incidence as in Fig. 4.

Fig. 8. Energy loss spectrum derivatives for 56 eV primary electrons from silicon (111) surface with 7x7 structure (Fig. 5b). Angle of incidence selected for optimizing details in spectrum.

Fig. 9. Primary electron energy dependence of 17.8 eV (dashed curve) and 15.2 eV (solid curve) amplitudes for Si(111)-7x7 structure (schematic); angle of incidence as in Fig. 4; normalized to constant primary current.

Fig. 10. $\varepsilon_2(\omega)$ and $\omega^2\varepsilon_2(\omega)$ for silicon, calculated[25] from PHILIPP and EHRENREICH's experimental data[26].

---

[26] PHILIPP, H.R., and H. EHRENREICH: Phys. Rev. 129, 1550 (1963).

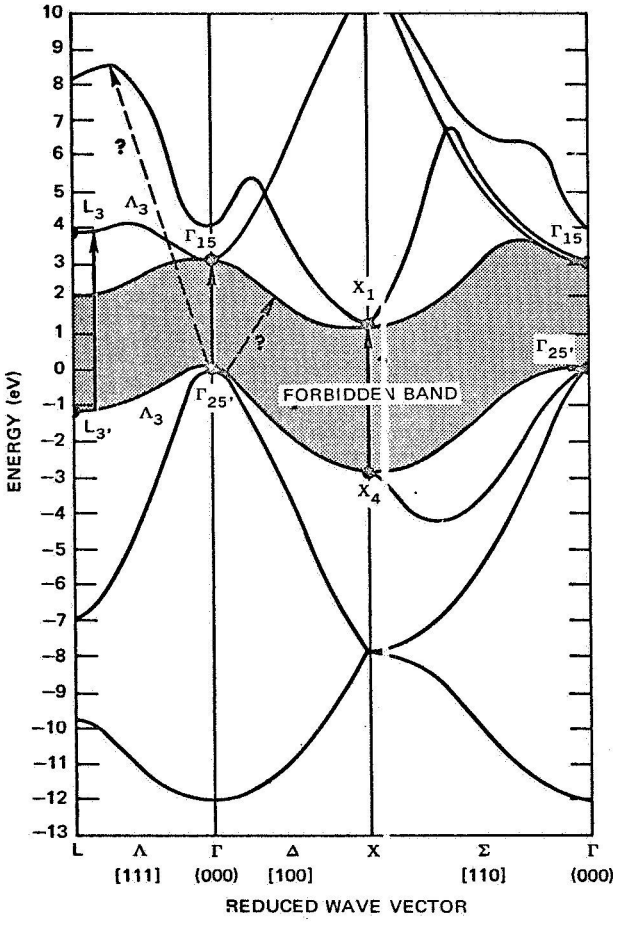
ENERGY (eV)
10
9
8
7
6
5
4
3
2
1
0
−1
−2
−3
−4
−5
−6
−7
−8
−9
−10
−11
−12
−13
L
Λ
[111]
Γ
(000)
Δ
[100]
X
Σ
[110]
Γ
(000)
REDUCED WAVE VECTOR
L3
Λ3
Γ15
X1
Γ25'
FORBIDDEN BAND
X4
L3'
Λ3
Γ25'
Γ15
?
?

Fig. 1

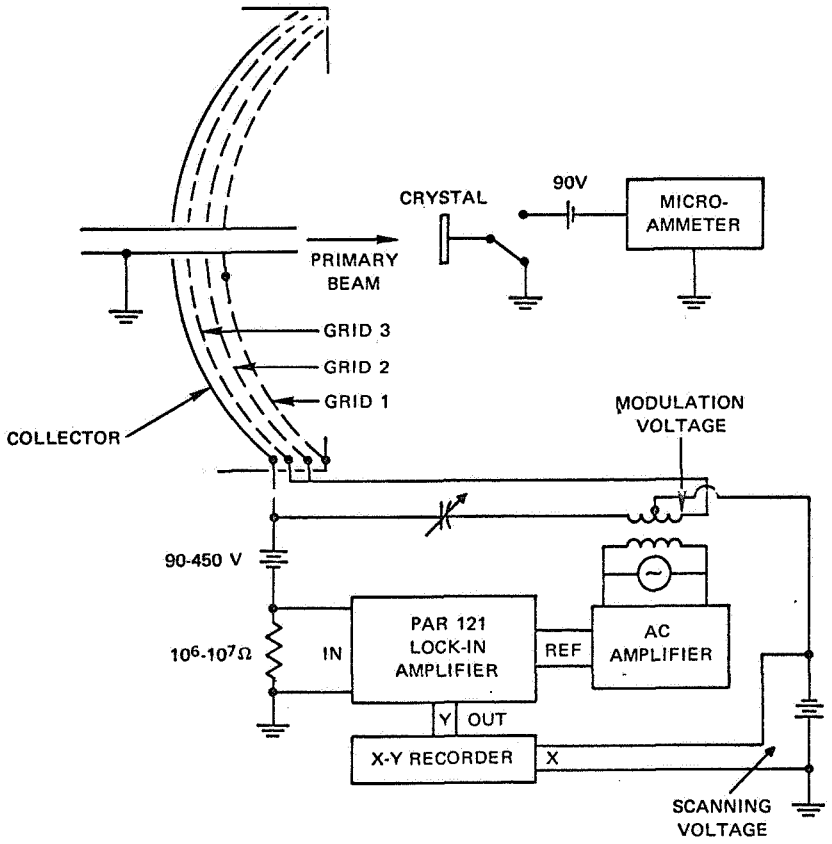
CRYSTAL
90V
MICRO-
AMMETER
PRIMARY
BEAM
GRID 3
GRID 2
GRID 1
COLLECTOR
MODULATION
VOLTAGE
90-450 V
10^6-$10^7\Omega$
IN
PAR 121
LOCK-IN
AMPLIFIER
REF
AC
AMPLIFIER
Y
OUT
X-Y RECORDER
X
SCANNING
VOLTAGE

Fig. 2

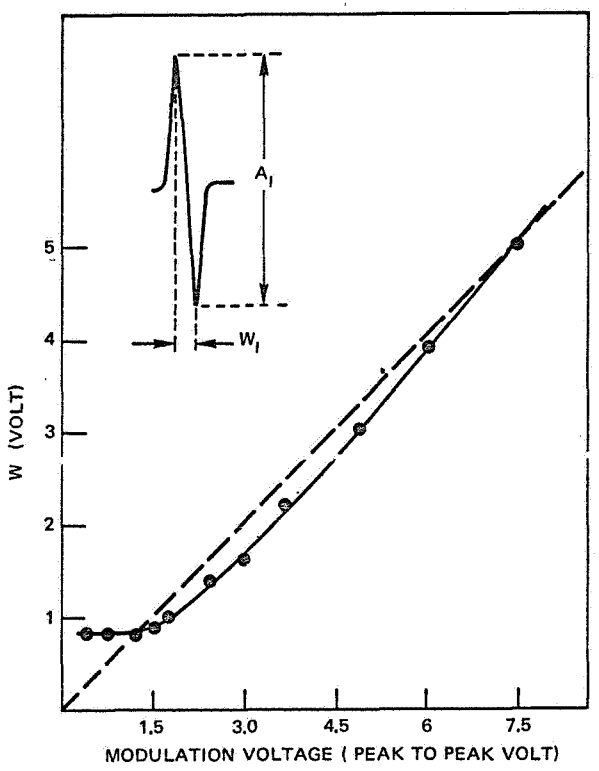
A1
W1
5
4
3
2
1
W (VOLT)
1,5
3,0
4,5
6
7,5
MODULATION VOLTAGE (PEAK TO PEAK VOLT)

Fig 3

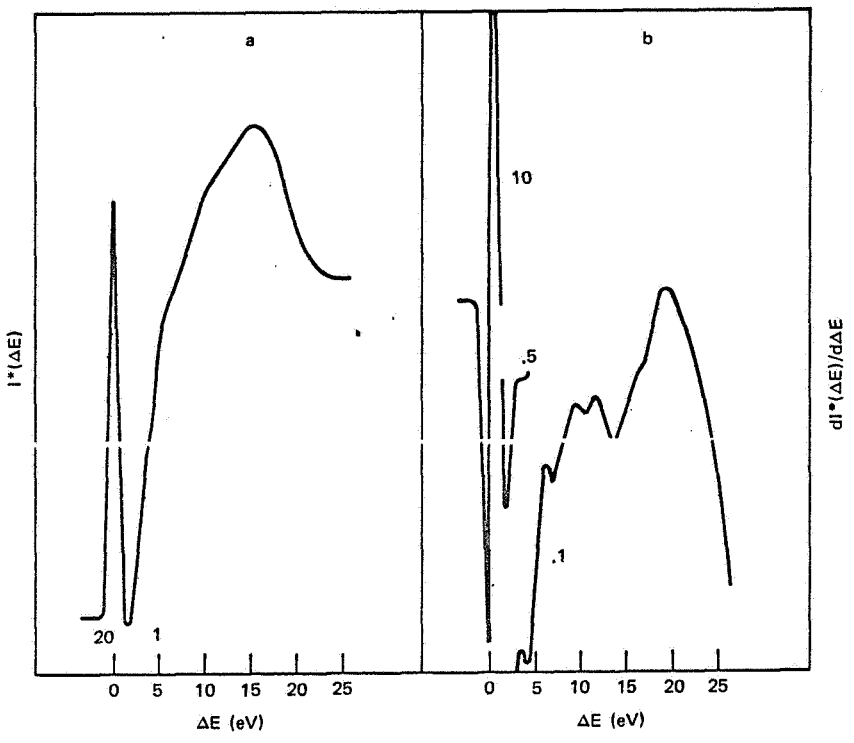

Fig 4

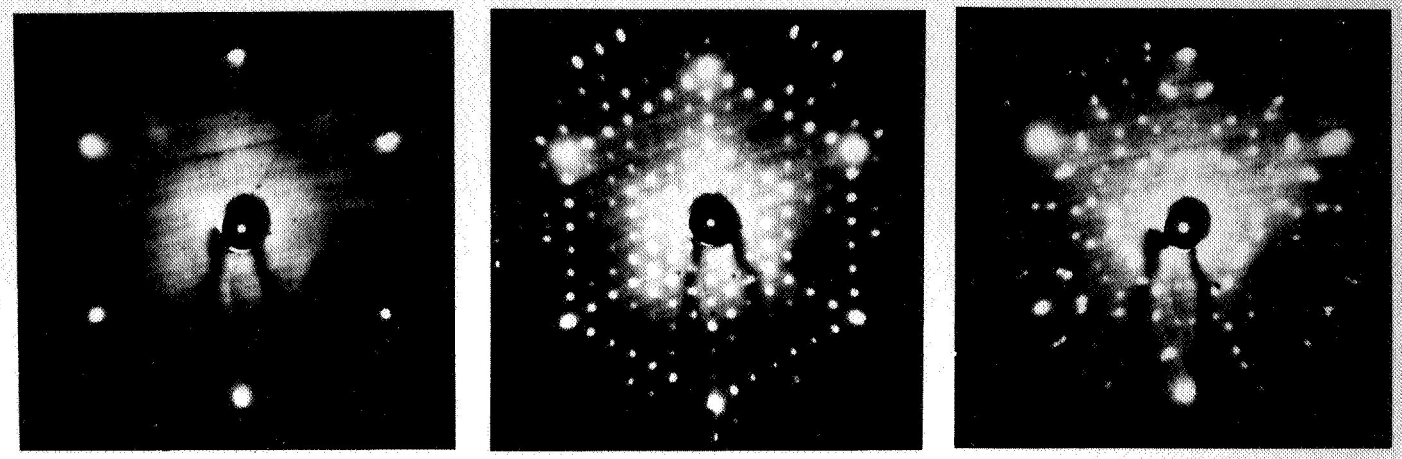

(a) (b) (c)

Fig. 5

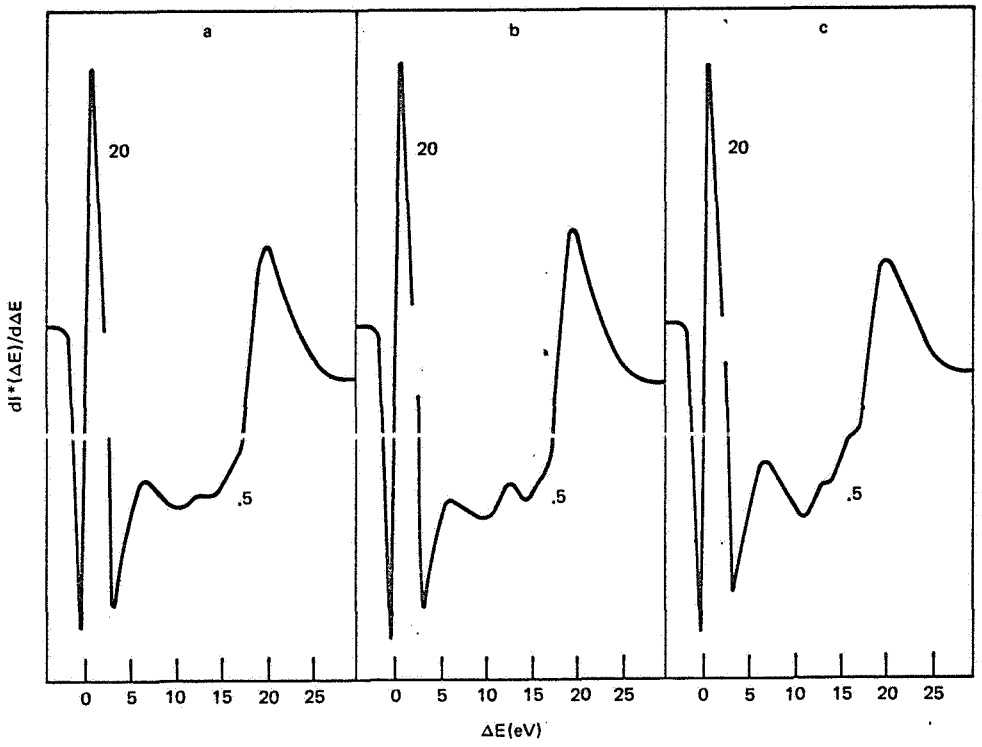
a
b
c
20
20
20
.5
.5
.5
0 5 10 15 20 25
0 5 10 15 20 25
0 5 10 15 20 25
dI*(ΔE)/dΔE
ΔE(eV)

Fig 6

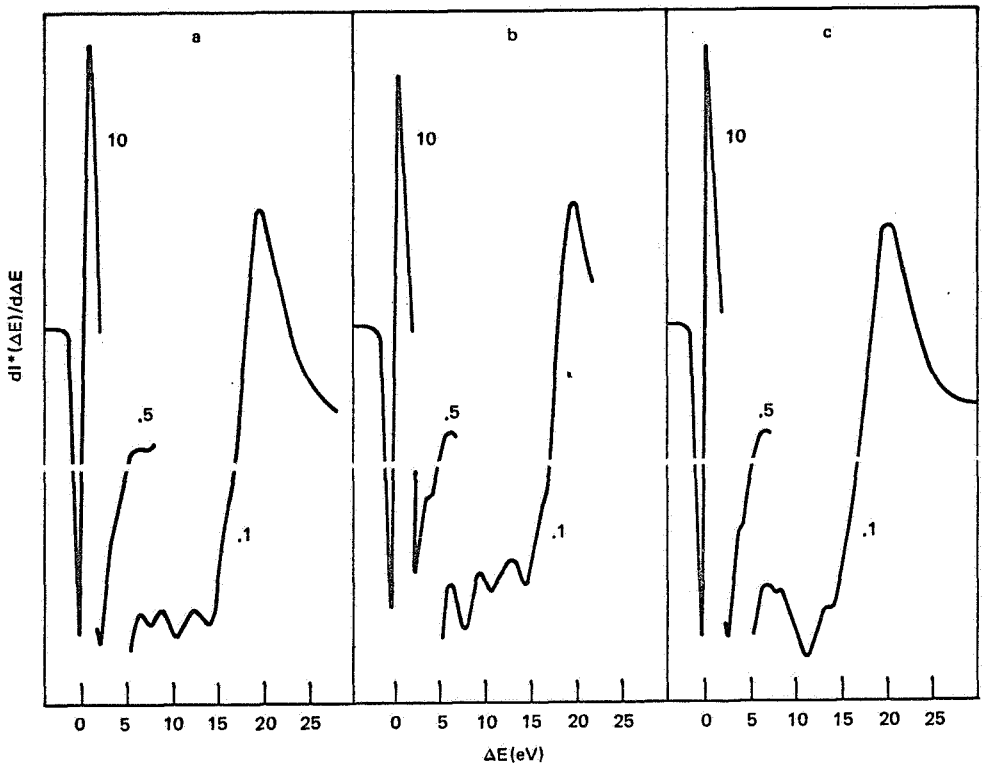

Fig. 7

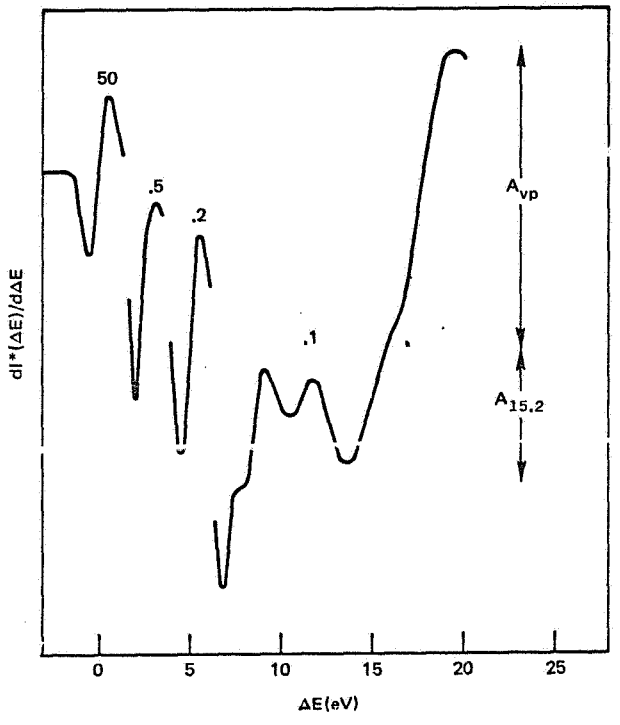

Fig. 8

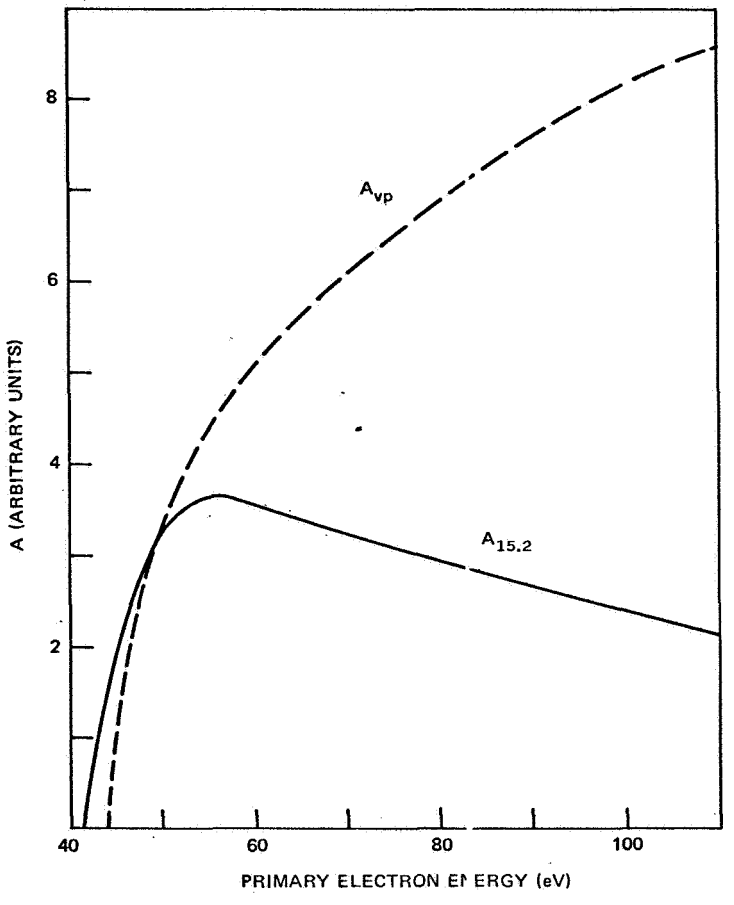
8
6
4
2
A (ARBITRARY UNITS)
A_{vp}
$A_{15.2}$
40
60
80
100
PRIMARY ELECTRON ENERGY (eV)

Fig. 9

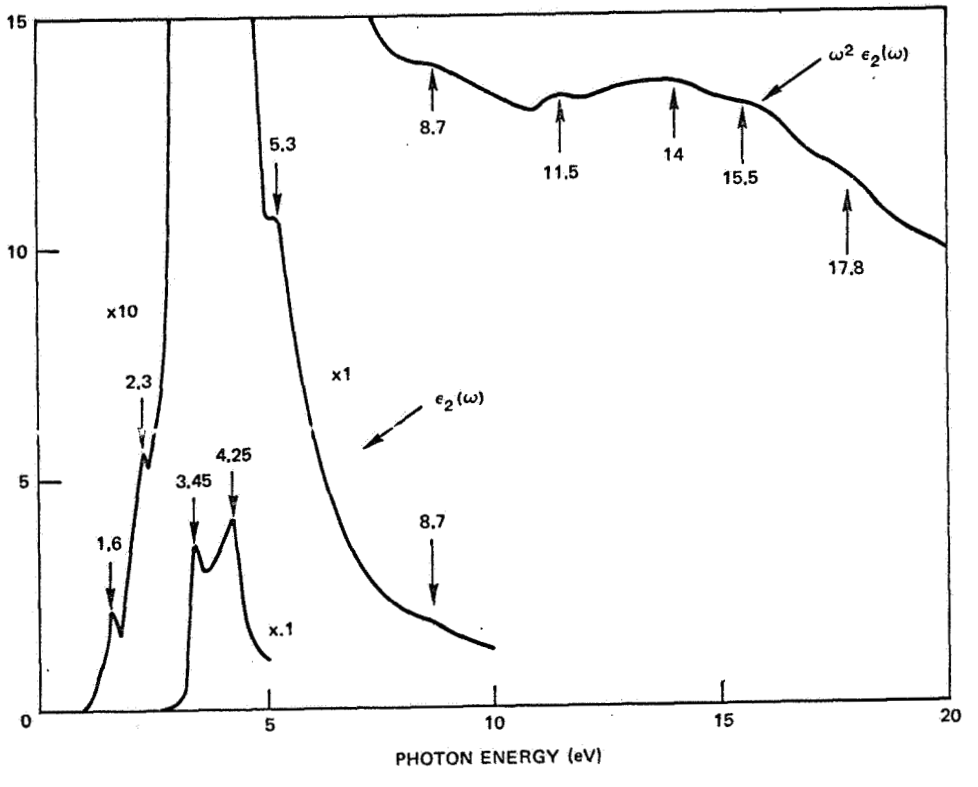
15
10
5
0
5
10
15
20
PHOTON ENERGY (eV)
$\omega^2 \epsilon_2(\omega)$
8.7
11.5
14
15.5
17.8
5.3
x10
2.3
1.6
3.45
4.25
x.1
x1
$\epsilon_2(\omega)$
8.7

Fig 10